A major purpose of the Technical Information Center is to provide the broadest dissemination possible of information contained in DOE's Research and Development Reports to business, industry, the academic community, and federal, state and local governments.

Although a small portion of this report is not reproducible, it is being made available to expedite the availability of information on the research discussed herein.

LA-UR--84-499

DE84 007504

TITLE A PRELIMINARY MODEL FOR HEAT TRANSPORT WITHIN A TONGUE-AND-RESERVOIR LIQUID DIODE FOR PASSIVE SOLAR HEATING

AUTHOR(S) G. F. Jones

SUBMITTED TO ASME/AIChE National Heat Transfer Conference
Niagara Falls, New York
August 5-8, 1984

DISCLAIMER

MASTER

Los Alamos National Laboratory
Los Alamos, New Mexico 87545

A PRELIMINARY MODEL FOR HEAT TRANSPORT WITHIN A TONGUE-AND-RESERVOIR LIQUID DIODE FOR PASSIVE SOLAR HEATING*

by

G. F. Jones
Solar Energy Section
Advanced Engineering Technology
Los Alamos National Laboratory
Los Alamos, New Mexico 87545

ABSTRACT

We present a preliminary model for heat transport within a tongue-and-reservoir liquid diode for passive solar heating. The diode consists of a rectangular vertical slot (tongue) extending from the bottom of a rectangular-shaped reservoir at the reservoir's front face. Water is used as the working fluid in the tongue and reservoir. Solar radiation is incident on the front face of the tongue, which also loses heat to the outside, while radiation and convection transport heat from the back of the reservoir to the building. Convection transports heat when the tongue is irradiated; however, when convection ceases and the temperature of the tongue cools below that of the reservoir (from exposure to the outside temperature), the reservoir stratifies, and the primary heat loss mechanism is conduction through the tongue and its fluid. The result is a passive solar component that may outperform most others. Flow in the tongue is treated as boundary layer flow; the integral forms of the governing equations are combined to form a single equation governing the local boundary layer thickness. The results are shown to depend upon the Grashof, Prandtl, and heat-loss Biot numbers. Results from this model agree well with those from our flow visualization experiments. We also propose a model for diode heat

*Work performed under the auspices of the US Department of Energy, Office of Solar Heat Technology.

transport processes during cool-down. In this model, an empirical coefficient accounts for the weak convective mixing that occurs in the reservoir during this phase. Preliminary results indicate the coefficient to be spatially dependent but independent of time and reservoir temperature. More experiments are planned to further validate both of the models described above.

I. INTRODUCTION

Recent analyses (Ref. 1) have shown that the performance of passive heating systems could be doubled by using more effective means of transporting passively collected solar energy to the building interior. Because of the large conversion efficiencies that result from such increases, the common constraint of utilizing only those surfaces that face the equator for solar collection no longer applies. It is conceivable that, with the whole surface area available for solar collection, we can work toward utilizing the entire envelope area of the building.

As a first step towards achieving this goal, we must investigate thermal transport mechanisms or devices that operate at equal or increased rates of solar collection and reduced rates of heat loss relative to those that are presently state-of-the-art.

Among the advanced thermal transport devices currently under study are thermal diodes*. Thermal diodes transport heat preferentially in one direction. Thus, heat that is collected at the surface of a building is transported efficiently to the inside, but heat cannot readily escape from the building along the same path.

We are presently investigating two types of thermal diodes. First is a two-phase (liquid-vapor) diode that transports heat by means of the working fluid's latent heat of evaporation from a hot surface (collector/boiler) to a cool one (condenser). A recent study by Hedstrom (Ref. 3 and personal communication) showed that such systems are capable of transporting heat downward a distance of about 5.5 m (18 ft) with overall system efficiencies of about 50%. The downward transport of heat is essential for the use of roof-mounted apertures.

The second, slightly less complicated type, is the liquid convective diode, which transports heat by means of a single-phase liquid by convective motion from a heated absorber surface to a higher-placed, cooler reservoir. Thus, the liquid convective diode performs as a collector and storage component in a single unit.

Convective diode geometries have been proposed by Jones (Ref. 4), Maloney (Refs. 5, 6, 7, and 8), Trefethen (Ref. 9), and Trefethen and Chung (Ref. 10). The geometry described in Ref. 10, investigated in more detail by Chung and Trefethen (Ref. 11), consisted of a stack of inclined flat plates bounded by a hot slab on one side and a cool one on the other. Here, the hot slab represents a collector surface and the cool slab, a heat exchange or energy storage device. The inclination angle of the plates generates a series of vertical cavities that slope upward from the hot to the cool slab. During heating, density imbalances within each cavity cause convective heat transfer from the collector to the heat exchanger or storage. However, when heating ceases and the collector is allowed to cool through heat loss to the outside temperature, the fluid layers within each cell become stable, and heat transport in the opposite direction is primarily by molecular conduction through the stacked plates and the stagnant working fluid.

The behavior described above is fundamental to all convective diode geometries; we note that convective diode operation consists of two distinct phases:* warm-up, where heat is transported to the diode from solar heating; and cool-down, where heat is transported from the diode to the outside. Further heat transport may occur to the building directly from hot surfaces of the diode during either of these two phases.

This paper concerns the analysis of heat transport processes in a type of liquid convective diode (hereinafter referred to as "diode"). Both experimental and analytical methods have been employed and preliminary performance models are proposed from theoretical considerations and from the results of the experiments.

A. Diode Description and Operation

The geometry for the diode under consideration, shown in Fig. 1, consists of a rectangular vertical slot (tongue) extending from the bottom of a rectangular-shaped reservoir at the reservoir's front face. Water is used as the working fluid in both the tongue and reservoir. In operation, solar radiation is incident on the front face of the tongue, which is also losing

heat to the outside by convection and infrared radiation. Simultaneously, radiation and convection heat transfer occur at the back face of the reservoir, which is exposed to the interior of the building. All other outer surfaces of the diode are insulated.

Within the diode, heat is transported by convection when the tongue is heated (warm-up phase). However, when convection ceases and the temperature of the tongue is reduced below that of the reservoir by ambient cooling (cool-down phase), the reservoir flow stratifies and conduction through the stagnant tongue fluid and the tongue itself occurs. Thus, it is the location of the tongue relative to the reservoir that supports stratification within the reservoir during cool-down, and it is stratification that causes the diode effect. Accordingly, heat losses to the outside are significantly reduced compared with what they would be if convection were to occur during this phase. We further note that within a conventional water wall, convection will always occur during nighttime cooling unless the wall is adequately insulated from outside temperatures. No movable insulation is required for the diode.

The diode geometry considered here is a variation of that proposed by Maloney (Refs. 6 and 7) and shown in Fig. 2. The latter configuration employs an offset between the front face of the reservoir and tongue, thus allowing many diodes to be stacked upon one another by fitting the tongue of one diode into the offset in the reservoir below it.* Such an arrangement utilizes nearly all available solar-aperture area and produces a smooth appearance of the diode stack from both inside and outside the building.

We believe that the heat transport processes that occur within the diode are not sensitive to the differences in geometry between the Maloney-proposed design and that which we are studying, provided the offset channel connecting the reservoir to the tongue is properly designed. Because this conclusion will become more apparent during discussion of the experimental results, no further justification will be given here.

B. Description of Experiments

To control the rate of heat input to the diode, the front face of the tongue (see Fig. 1) was fitted with a strip-heated copper plate 0.45 m^2 (4.85 ft^2) in area and 1.65 mm (0.065 in.) thick. The strip heaters were placed on 7 cm (2.75 in.) centers to provide heat flux on the inside surface

of the tongue uniform to within 3% as determined by a method developed by Jones (Ref. 12). The strip heaters are capable of supplying heat fluxes of up to 1 kW/m^2 to the tongue flow controllable by a variable AC power transformer.

A rake supporting 27 copper-constantan thermocouples (11 in the reservoir and 16 in the tongue) was installed in the diode as shown in Figs. 3 and 4. Data from these sensors together with ambient temperature and heater-plate temperature were automatically scanned during warm-up once every 30 seconds for the first 20 minutes of the experiment, and once every minute thereafter at a rate that varied from 1 channel per second to 15 channels per second. Power dissipated by the strip heaters was held constant during any single warm-up experiment and was recorded manually.

During the warm-up phase, the entire outer surface of the diode, except for the back face of the reservoir, was covered with polystyrene insulation a minimum of 7.6 cm (3 in.) thick. A layer 15.2 cm (6 in.) thick was applied to the heating-plate surface area. During cool-down, the insulation covering the heating plate was removed and power to the heating plate turned off simultaneously.

In addition to temperature measurements, flow-visualization experiments were also performed using high-impact polystyrene beads of 0.1 mm (0.078 in.) nominal size and having a specific gravity of about 1.04. A small amount of salt was added to the water in the diode to bring the beads to a neutrally buoyant condition. Videotaping of selected experiments was performed for future reference.

C. Heat Transport Analysis

1. Warm-up Phase. Past studies of natural convection in large-aspect-ratio vertical slots of the type by Elder (Ref. 13); Buchberg, Catton, and Edwards (Ref. 14); and Randall, Mitchell, and El-Wakil (Ref. 15) apply to a totally confined geometry and not to the present geometry of an open-ended tongue. Because of the lack of an upper-end effect in our case and under the guidance of preliminary flow-visualization results to be discussed later, we theorize fluid motion within the tongue to be boundary layer-like; that is, one boundary layer results from the fluid rising adjacent to the heated tongue surface and another one results from the descending flow on the cool, opposite face of the tongue. This behavior is clearly expected under the conditions of large tongue thicknesses and small-to-moderate heating

rates; for in these cases, a nonconvective core exists such that no momentum transport between the rising and falling flows is possible. For the present analysis, the effect of momentum transport between the opposing boundary layer flows is neglected.

We further assume that energy storage rates during warm-up are small relative to the convective heat transfer rates, so that heat-transport processes during this phase may be treated as quasi-steady. All fluid properties are also assumed to be constant in this analysis and the next.

Consider the boundary layer flow of water over the irradiated tongue of a diode that also loses heat to the outside by radiation and convection. The situation is depicted in Fig. 5. The geometry and other variables used in this and the following analysis are given in Fig. 6.

The integral forms of the boundary layer equations are written as

$$\frac{d}{dx} \int_0^\delta u^2 \, dy = -\nu \left. \frac{\partial u}{\partial y} \right|_{y=0} + \int_0^\delta g\hat{\beta}(T - T_\infty) \, dy \tag{1}$$

$$\frac{d}{dx} \int_0^\delta u(T - T_\infty) \, dy = -k \left. \frac{\partial T}{\partial y} \right|_{y=0} . \tag{2}$$

These equations may be integrated and solved simultaneously after establishing generalized shapes of the velocity and temperature profiles. This is done in the usual way (see Ref. 16) by assuming a quadratic temperature profile and a cubic velocity profile and evaluating all of the coefficients except one from the available boundary conditions. Thus, we assume here

$$T - T_\infty = A_0 + A_1 y + A_2 y^2 , \tag{3}$$

$$u = B_0 + B_1 y + B_2 y^2 + B_3 y^3 . \tag{4}$$

The boundary conditions for this situation are

$$T(x,\ y = \delta) = T_\infty \quad , \tag{5a}$$

$$\left.\frac{\partial T}{\partial y}\right|_{y = \delta} = 0 \quad , \tag{5b}$$

$$-k \left.\frac{\partial T}{\partial y}\right|_{y = 0} = q - U_L\ [T(x,\ y = 0) - T_a] \tag{5c}$$

and

$$u(x,\ y = 0) = 0 \quad , \tag{6a}$$

$$u(x,\ y = \delta) = 0 \quad , \tag{6b}$$

$$\left.\frac{\partial u}{\partial y}\right|_{y = 1} = 0 \quad , \tag{6c}$$

$$\nu \frac{\partial^2 u}{\partial y^2} = -g\hat{\beta}\ [T(x,\ y = 0) - T_\infty] \quad . \tag{6d}$$

Eq. (6d) results from the boundary layer form of the momentum equation written at the tongue wall.

Eqs. (3) and (4) become with Eqs. (5) and (6)

$$T - T_\infty = \frac{\hat{q}\ \delta\ (1 - \eta)^2}{2k\ [K\delta + 1]} \quad , \tag{7}$$

where

$$\hat{q} \equiv q + U_L(T_a - T_\infty) \quad ,$$

$$K \equiv U_L/k \quad ,$$

$$\eta \equiv y/\delta \quad ,$$

and

$$\frac{u}{u_x} = \eta(1 - \eta)^2 \quad , \tag{8}$$

repectively. Here, u_x is an unknown function of x as is the local boundary layer thickness, δ. These will be determined from the solution of Eqs. (1) and (2). In arriving at Eq. (8), the relationship

$$u_x \sim \frac{\delta^3}{K\delta + 1} \tag{9}$$

also holds.

Combining Eqs. (7) and (8) with Eqs. (1) and (2), integrating each and eliminating the proportionality constant [implied by Eq. (9)] between them, we obtain the dimensionless form of the governing equation for the local boundary layer thickness

$$\frac{d\hat{\delta}}{d\hat{x}} - \frac{360\ (Bi\ \hat{\delta} + 1)^2}{Pr\ Gr_L^*\ (3\ Bi\ \hat{\delta}^5 + 5\hat{\delta}^4)} \left\{ 1 + \frac{4(1 + \frac{5}{7}\ Bi\ \hat{\delta})}{5Pr(1 + \frac{3}{5}\ Bi\ \hat{\delta})} \right\} = 0 \quad , \tag{10}$$

where

$$\hat{\delta} \equiv \delta/L \quad ,$$

$$\hat{x} \equiv x/L \quad ,$$

$$Bi \equiv LU_L/k \quad \text{(Biot number)} \quad ,$$

$$Gr_L^* \equiv g\hat{\beta}\,\hat{q}\,L^4/\kappa\nu^2 \quad \text{(Grashof number)} \quad ,$$

$$Pr \equiv \nu/\kappa \quad \text{(Prandtl number)} \quad ,$$

and the initial condition $\hat{\delta}\,(\hat{x} = 0) = \hat{\delta}_i$ is determined from experiments.

Once Eq. (10) is solved for the boundary layer thickness, the local temperature and velocity profiles are determined from Eqs. (7) and (8), respectively. Additional local and integrated heat-transfer and fluid-flow results may then be obtained directly from these values.

Most significant among these results is an expression for the integrated thermal performance of the diode as a solar collector. A steady energy balance on the tongue of the diode gives

$$q_a(x) = q - U_L\,[T(x,\ y = 0) - T_a] \quad , \tag{11}$$

where $q_a(x)$ is the net local heat flux on the tongue surface. After nondimensionalizing, substituting Eq. (7) and integrating, we obtain an expression for the instantaneous thermal efficiency of the diode tongue as

$$E = \left[(\alpha\tau)_e - \frac{U_L}{I}\,(T_\infty - T_a)\right] \left\{1 - \frac{Bi}{2} \int_0^1 \frac{\hat{\delta}\,d\hat{x}}{(Bi\,\hat{\delta} + 1)}\right\} \quad . \tag{12}$$

We note that Eq. (12) is in the same form as the conventional Hottel-Whillier-Bliss (HWB) expression for the instantaneous efficiency of a flat plate collector (Ref. 17) with the term in the curly brackets denoted as the "collector heat removal factor," F_{RD}. Thus, for a diode

$$F_{RD} = 1 - \frac{Bi}{2} \int_0^1 \frac{\hat{\delta}\, d\hat{x}}{(Bi\ \hat{\delta} + 1)} .$$

One notable difference here, however, is that F_R for a flat plate collector is nearly constant for a given system, whereas for a diode it is a function of fluid properties (which, over long time periods, depend on temperature) and, more importantly, rate of heat input to the diode tongue. This result is a direct consequence of the fact that forced convection is usually employed in systems using flat plate collectors, whereas natural convection driven by heat input to the tongue is the heat transport mechanism in diodes.

We further note that for any nonzero value of Bi, Eq. (12) predicts reduced values of efficiency for increased boundary layer thicknesses. This result is in agreement with the explanation that because the boundary layer is the distance over which the fluid temperature is greater than T_∞, thicker boundary layers produce higher temperatures at the tongue surface than to thinner ones. Higher surface temperatures increase the rate of heat loss and thus reduce diode efficiency.

Turning attention to the reservoir temperature, T_∞, in Eq. (12), we expected and experimentally verified that even at low rates of heating of the diode tongue, the vigorousness of convection within the reservoir from the rising tongue flow is sufficient to cause the reservoir to operate at near-isothermal conditions at any instant in time. Thus, T_∞ is determined by solving a lumped energy balance on the diode accounting for the energy inflow at the tongue, the energy outflow at the reservoir's back, and energy storage. This balance is solved iteratively with Eq. (12) to obtain the correct values of E and T_∞.

It is of further interest here to examine Eq. (10) for the limiting case of no heat loss to the outside. For this case, the solutions from Eq. 10 may be compared with the results obtained from the experiments, for in these, the heat flux supplied to the tongue is known.

Eq. (10) becomes

$$\frac{d\hat{\delta}}{d\hat{x}} - \frac{72\left(1 + \frac{4}{5Pr}\right)}{Pr\ Gr_L^*\ \hat{\delta}^4} = 0 \quad ,$$

and may be integrated immediately to obtain

$$\hat{\delta} = (360)^{1/5}\ Pr^{-2/5}\ \left(\frac{4}{5} + Pr\right)^{1/5}\ Gr_L^{*\ -1/5} \quad . \tag{13}$$

From Eqs. (8) and (9), the maximum velocity within the boundary layer occurs at $y = \delta/3$ and for the location $x = L$, it may be written as

$$U_{max} = \frac{80k}{9L}\ (360)^{-2/5}\ Pr^{4/5}\ \left(\frac{4}{5} + Pr\right)^{-2/5}\ Gr_L^{*2/5} \quad . \tag{14}$$

2. Cool-down Phase. A short time after heating of the tongue ceases, convection in the tongue and the vigorous convective mixing within the reservoir caused by fluid motion in the tongue stop. The latter heat transport mechanism is replaced by a weak convective motion in the reservoir caused by two simultaneously occurring, independent effects.

The first effect is the result of convective cooling of the reservoir fluid adjacent to the back face of the reservoir caused by heat transport to the building. The direction of this motion is down at the back face of the reservoir and up through the remainder of the reservoir's horizontal cross section.

The second effect results from cooling of the reservoir from below by the tongue. Because the area for this cooling is of width, t, and the reservoir is of a larger width, d, the cooling process attempts to establish horizontal temperature gradients within the reservoir. Convection occurs because the fluid cannot support these gradients. We believe (although it is not as yet verified) that this convection is cellular in nature because the magnitudes of the effects of convection and conduction are of equal order.

As a first approximation to a more detailed model, we will assume here that all effects in the reservoir that occur in the y_∞ direction may be lumped. The motivation for this assumption is the absence of any y_∞-direction temperature gradients here, as discussed above. Thus, the heat-conduction term in the reservoir model becomes one dimensional (in the x_∞ direction) and acts through an area of width, t. The energy storage term accounts for all the energy stored in the reservoir fluid of width, d. A term accounting for heat transport within the reservoir caused by the weak mixing described above is included in the model and employs an empirical convection coefficient.

Finally, because of the thinness of the tongue, the tongue model also includes the assumption that conduction in the y direction is lumped.

Subject to the above conditions, the dimensionless form of the energy balance for the reservoir becomes

$$\frac{\partial \psi_\infty}{\partial \tau} = \lambda \frac{\partial^2 \psi_\infty}{\partial \eta_\infty^2} - \gamma^2 \, Nu_m \, \psi_\infty \quad , \tag{15}$$

where $\psi_\infty \equiv \dfrac{T_\infty - T_b}{T_i - T_b}$, $\eta_\infty \equiv \dfrac{x_\infty}{\ell}$, $\lambda \equiv \dfrac{t}{d}$,

$\tau \equiv \dfrac{\tau^* K}{\ell^2}$, $\gamma \equiv \dfrac{\ell}{d}$, $Nu_m \equiv \dfrac{U_m d}{k}$.

Nu_m accounts for energy transport within the reservoir caused by weak convective mixing and is determined from experiments.

The boundary conditions for this problem are an insulated condition at the reservoir top and a condition that matches the reservoir temperature with the tongue temperature at the location where the reservoir and tongue meet. Thus, the boundary conditions and initial condition become

$$\left.\frac{\partial \psi_\infty}{\partial \eta_\infty}\right|_{\eta_\infty = 0} = 0 \quad , \quad \psi_\infty (\eta_\infty = 1, \tau) = a\psi (\eta = 1, \tau) + b \quad , \tag{16a}$$

and $$\psi_\infty (\eta_\infty, \tau = 0) = 1 \quad . \tag{16b}$$

Here $$a \equiv \frac{T_i - T_a}{T_i - T_b} \quad , \quad b \equiv \frac{T_a - T_b}{T_i - T_b} \quad . \tag{16c}$$

Eq. (15) is solved by the usual methods of superposition and separation of variables to obtain the reservoir temperature distribution.

$$\psi_\infty (\eta_\infty, \tau) = \frac{b \cosh \mu \eta_\infty}{\cosh \mu} +$$

$$2 \sum_{j=0}^{\infty} \left\{ \frac{(-1)^j}{(j + 1/2)\pi} - \frac{b[(j + 1/2)\pi (-1)^j - \mu \tanh \mu]}{\mu^2 + (j + 1/2)^2 \pi^2} \right\}$$

$$\cdot e^{-\nu_\infty \left(\frac{}{}\right)^2 \tau} \cos (j + 1/2)\pi \eta_\infty$$

$$+ a\psi\ (\eta = 1,\ \tau) \quad ,$$

$$\cdot \left\{ \frac{\cosh \mu \eta_\infty}{\cosh \mu} - 2 \sum_{i=0}^{\infty} \frac{(i + 1/2)\ \pi\ (-1)^i - \mu \tanh \mu}{\mu^2 + (i + 1/2)^2\ \pi^2} \right.$$

$$\left. e^{-\nu_{\infty i}^2 \tau} \cos\ (i + 1/2)\pi\eta_\infty \right| \quad , \tag{17}$$

where $\nu_{\infty j}^2 \equiv (j + 1/2)^2\ \pi^2\ \lambda + \gamma^2\ Nu_m$, etc.,

and $\mu^2 \equiv \dfrac{\gamma^2\ Nu_m}{\lambda}$.

In Eq. (17) both series terms represent the transient portion of temperature distribution that are dominant for small periods of elapsed ime. The remaining terms in Eq. (17) represent the steady-state temperature distribution that persists after long periods of cool-down time have elapsed.

The dimensionless form of the energy balance for the tongue is written as

$$\frac{\partial \psi}{\partial \tau} = \beta^2 \frac{\partial^2 \psi}{\partial \eta^2} - \beta^2 \alpha\ Nu_f\ \psi \quad , \tag{18}$$

where $\psi \equiv \dfrac{T - T_a}{T_i - T_a}$, $\eta \equiv \dfrac{x}{L}$, $\beta \equiv \dfrac{\ell}{L}$,

$$\alpha \equiv \frac{L}{t} \ , \quad Nu_f \equiv \frac{U_f L}{k} \ .$$

The β^2 term appears in Eq. (18) because the time scaling for this analysis is the same as it is for the reservoir analysis, whereas the length scales are different.

Here, the boundary conditions are an insulated condition at the tongue bottom and a condition that matches the heat flux from the reservoir to that into the tongue at the location where the reservoir and tongue meet. The latter condition in comoination with the matching of temperatures at the tongue and reservoir interface ensures that both heat flux and temperature continuity from the reservoir to the tongue are maintained.

The boundary conditions and initial condition become

$$\left.\frac{\partial \psi}{\partial \eta}\right|_{\eta = 0} = 0 \quad , \quad \left.\frac{\partial \psi}{\partial \eta}\right|_{\eta = 1} = -q_L / q_n \quad , \tag{19a}$$

and $\psi(\eta, \tau = 0) = 1$. (19b)

Here q_L is the dimensional heat flux from the reservoir to the tongue, and q_n is a normalizing heat flux defined by

$$q_n \equiv \frac{k}{L} (T_i - T_a) \quad .$$

We again employ superposition and separation of variables to obtain the tongue temperature distribution.

$$\psi(\eta, \tau) = 1 + \frac{q_L}{\nu^2 q_n} \left\{ 1 - \frac{\nu \cosh \nu\eta}{\sinh \nu} + 2 \sum_{n=1}^{\infty}{}' \frac{(-1)^n}{\nu^2 + n^2\pi^2} e^{-\lambda_n^2 \tau} \cos n\pi\eta \right\} \quad , \tag{20}$$

where $\lambda_n^2 \equiv (n\pi\beta)^2 + \beta^2 \alpha Nu_f$,

and $\nu^2 \equiv a\ Nu_f$.

The Fourier series Eqs. (17) and (20) are solved simultaneously* to obtain the final temperature distributions in the reservoir and tongue, respectively. Expressions for heat-transfer rates and thermal performance of the diode during cool-down are then obtained directly from these solutions.

II. RESULTS AND DISCUSSION

A. Flow-Visualization Experiments

Two experiments using high-impact polystyrene beads as flow-visualization media were performed. In the first experiment, the tongue was heated at a rate of 750 W/m^2 (high-flux case), and in the second, at a rate of 250 W/m^2 (low-flux case).

For the high-flux case, we noted that the upflowing stream from the tongue traveled along the diode's front face until it reached the free surface at the top of the reservoir. At this location it turned, moved along the free surface for some short distance and began its descent. The thickness of the rising layer of fluid in the reservoir was about 1 cm (0.39 in.) and did not appear to thicken with distance traveled. The remainder of the reservoir fluid that was not involved in the upflow moved downward slowly, where, upon approaching the entrance to the tongue, it accelerated very rapidly. The boundary-layer thicknesses in the tongue were about 0.65 cm (0.25 in.) for the upflow and about twice that for the downflow. The upflow velocity was measured at about 1.7 cm/s (0.67 in./s). Little, if any, interaction between the two opposing streams in the tongue was noted. The flow appeared to be laminar and two dimensional throughout. In addition, we could not detect any evidence of flow separation as the flow from the reservoir entered the tongue. Quasi-steady conditions were reached after about 10 minutes of heating for this experiment.

After about 1 hour of heating, results from the low-flux case experiment were similar to those of the high-flux case. The upflow velocity at the top of the tongue was about 1.1 cm/s (0.43 in./s) and the boundary-layer thicknesses were approximately those of the high-flux case. Before 1 hour of heating had elapsed, the upflow from the tongue penetrated only a fraction of

the distance into the reservoir before it cooled, turned away from the wall, and descended. We noted the penetration depth of the upflowing stream into the reservoir to increase with time, as expected. Again, no strong interaction between the opposing fluid streams in the tongue was detected.

A comparison between the calculated and measured boundary-layer thicknesses and velocities within the tongue at $x = L$ for the two experiments is presented in Table I. The results indicate agreement to within 12% for boundary-layer thickness and closer agreement for velocity. We feel that the good agreement validates the model for the data obtained. We further note, by inspecting Eq. (7), that because the fluid temperature is nearly proportional to the boundary-layer thickness, similar good agreement should occur between the measured and calculated temperature distribution. More experiments are planned to validate this supposition.

TABLE I

COMPARISON OF CALCULATED RESULTS FROM EQS. (13) AND (14) WITH THOSE FROM THE FLOW VISUALIZATION EXPERIMENTS

Heating Rate (W/m^2)	Gr_L^*	δ_{calc} (cm)	δ_{meas} (cm)	$u_{max_{calc}}$ (cm/s)	$u_{max_{meas}}$ (cm/s)
750	1×10^{11}	0.57	0.65	1.56	1.7
250	3×10^{10}	0.72	~0.65	0.96	1.1

B. Temperature Histories

To date, we have performed several experiments to determine the thermal behavior of the reservoir during the warm-up and cool-down phases of operation.

Time/temperature histories at eight locations within the reservoir (see Fig. 3 for the location of each thermocouple number) during a 750 W/m^2 warm-up experiment are shown in Fig. 7. We note the agreement of all temperatures to within 1°C. When this experiment was performed, the voltmeter/scanner component of the data-acquisition system was capable only of resolving temperature to within 0.5°C. We feel that part of the 1°C difference in Fig. 7 is caused by this inaccuracy and that the actual difference is probably closer to 0.5°C. From the results shown in Fig. 7, we

also note that the assumption of a well-mixed reservoir during warm-up is quite accurate and thus the initial conditions, Eqs. (16b) and (19b), are validated.

The time/temperature histories at five horizontal locations within the reservoir during a 12-hour cool-down experiment are shown in Fig. 8. Here, temperature gradients in the horizontal direction are seen to be small or nonexistent, as was expected, because of the convective mixing within the reservoir during this phase.

Calculated [from Eq. (17)] and experimental time/temperature histories at four vertical locations within the reservoir are compared in Fig. 9. Here, T_b and T_a were maintained at about a constant 24°C; the initial reservoir temperature was uniform at about 44°C. The symbols *, #, @, and & represent calculated temperatures and the solid lines represent experimental data. In the calculations, the convection coefficient, Nu_m, was assigned the values of 1.6, 1.9, 1.9, and 0.5 at the four vertical locations, respectively, starting at the uppermost location. From inspection of Fig. 9, we note that the reservoir-fluid temperature, as expected, stratifies increasingly with time. We also note very good agreement (differences of less than 0.5°C) between the calculated results and the data, the good agreement persisting throughout the duration of the experiment. Thus, we suspect that Nu_m depends only on vertical location within the reservoir and possibly reservoir geometry but not on time or temperature differences within the reservoir or between the reservoir and its environment.

III. CONCLUSIONS

The warm-up and cool-down phases of operation of a convective liquid diode have been analyzed by experiments and theory. Reasonbly good agreement is obtained between the results from several experiments and those from relatively simple analytical models; however, further validation of the models is needed. At this stage of research, it appears that, because of the vigorous rate of convective heat transport during warm-up and the diminished rate of heat loss during cool-down, a well-designed liquid convective diode should be able to outperform most other passive heating components.

Along with model validation and refinement, the issues of diode materials and manufacturing must be addressed. In particular, it is essential for good diode performance to minimize the thermal resistance through the front face of

the tongue and the back face of the reservoir while maintaining large thermal resistances through the remaining surfaces. Also, uniform material thicknesses in the tongue are critical in maintaining a uniformly thick flow passage to ensure proper flow through it and good performance.

ACKNOWLEDGMENTS

Acknowledgments are due J. Tafoya, J. Hauser, and B. Ketchum, who assisted in building and instrumenting the experimental facilities, and J. C. Hedstrom and L. Dalton, who assisted with the data-acquisition system. This paper was typed by Jan Sander and edited by Sherry Reisfeld.

REFERENCES

1. D. A. Neeper and R. D. McFarland, "Some Potential Results of Fundamental Research for the Passive Solar Heating and Cooling of Buildings," Los Alamos National Laboratory report LA-9425-MS (August 1982).

2. S. Buckley, "Thermic Diode Solar Panels for Space Heating," Solar Energy 20, pp. 495-503 (1978).

3. J. C. Hedstrom, "Vapor-Phase Heat-Transport System," Passive and Hybrid Solar Energy Update Meeting, Washington, D.C., September 26-28, 1983. (LA-UR-83-2646)

4. G. F. Jones, "Quasi-Steady Heat Transport Within a Vertical-Tube-Array Liquid Diode," Los Alamos National Laboratory report (in preparation).

5. T. J. Maloney and G. S. Wattles, "Report on Tests of a Passive Phase Change Solar Diode for Space Heating," Progress in Solar Energy, AS/ISES, 205B McDowell Hall, University of Delaware, Newark, Delaware 97111, pp. 803-808 (1982).

6. T. J. Maloney, "Omnibus Thermal Storage Modulator System - Final Report - Draft," prepared for the US DOE Marketable Products for Passive Solar Applications Program under cooperative agreement, DE-FC02-80CS3 0526 (November 1981)

7. T. J. Maloney, One-Design, Inc., personal communication, December, 1982.

8. T. J. Maloney, One-Design, Inc., unpublished data, May 1982.

9. L. M. Trefethen, "Natural Convection Inside Inclined Tubes," Proc. Fourth Int. Heat Transfer Conf., Paris, September 1970 (Elsevier Publishing Co., Amsterdam, 1970) Paper 69-IC-189.

10. L. M. Trefethen and K. C. Chung, "The Oneway Heat Wall - Analysis and Experiments on a Vertical Stack of Inclined Cavities," Proc. Sixth Annual Heat Transfer Conf., Toronto, 1978 ( ), Vol. 4.

11. K. C. Chung and L. M. Trefethen, "Natural Convection in a Vertical Stack of Inclined Parallelogrammic Cavities," Int. J. Heat and Mass Transfer 25, pp. 277-284 (1982).

12. G. F. Jones, "Temperature and Heat-Flux Distributions Within a Strip-Heated Composite Slab," submitted for presentation at the 1984 ASME/AIChE National Heat Transfer Conference, Niagara Falls, New York, August 1984.

13. J. W. Elder, "Laminar Free Convection in a Vertical Slot," J. Fluid Mechanics 23, Part 1, pp. 77-98 (1965).

14. H. Buchberg, I. Catton, and D. K. Edwards, "Natural Convection in Enclosed Spaces - A Review of Application to Solar Energy Collection," J Heat Transfer 98, pp. 182-188 (1976).

15. K. R. Randall, J. W. Mitchell, and M. M. El-Wakil, "Natural Convection Heat Transfer Characteristics of Flat Plate Enclosures," J. Heat Transfer 101, pp. 120-125 (1979).

16. J. P. Holman, Heat Transfer (McGraw Hill Publishing Co., New York, 1976), pp. 236-241.

17. J. A. Duffie and W. A. Beckman, Solar Energy Thermal Processes (John Wiley and Sons, New York, 1974) p. 147.

NOMENCLATURE

a	$(T_i - T_a)/(T_i - T_b)$
b	$(T_a - T_b)/(T_i - T_b)$
A, B	Constants in Eqs. (3) and (4)
Bi	Biot number, LU_L/κ, dimensionless
d	Depth of reservoir, cm
E	Thermal efficiency, dimensionless
F_R	Collector heat-removal factor, dimensionless
g	Acceleration of gravity, m^2/s
Gr_L^*	Modified Grashof number, $g\beta\hat{q}L^4/\nu^2\kappa$, dimensionless
I	Insolation incident on glazing covering diode tongue, W/m^2
κ	Thermal conductivity, W/cm-K
K	U_L/κ, cm^{-1}
ℓ	Reservoir height, cm
L	Tongue height, cm
Nu_m	Empirical heat-loss coefficient in Eq. (15), dimensionless
Pr	Prandtl number, ν/κ, dimensionless
q	Heat flux at inside of tongue surface from irradiation of this surface, W/m^2
$\hat{q}$	$q + U_L (T_a - T_\infty)$, W/m^2
q_a	Net heat flux at inside of tongue surface, W/m^2
T	Temperature, °C
τ	Tongue thickness, cm
u	x-component of velocity in tongue, cm/s
u_{max}	Maximum x-component of velocity in tongue, cm/s
u_x	Characteristic velocity in tongue defined by Eq. (9), cm/s
U_L	Loss coefficient from inside front surface of tongue to ambient, W/cm^2-K

U_b Loss coefficient through the back surface of the reservoir, $W/cm^2 \cdot K$

x Vertical coordinate, cm

y Horizontal coordinate

Greek Symbols

α L/τ, dimensionless

$(\alpha\tau)_e$ Effective absorptance-transmittance of glazing and absorber surface on tongue, dimensionless

$\hat{\beta}$ Coefficient of thermal expansion for water, dimensionless

β ℓ/L, dimensionless

γ ℓ/d, dimensionless

δ Instantaneous boundary-layer thickness, cm

η Vertical coordinate, dimensionless

κ Thermal diffusivity, cm^2/s

λ t/d, dimensionless

μ $(\gamma^2 \, Nu_m/\lambda)^{1/2}$, dimensionless

ν Kinematic viscosity, cm^2/s

τ $\tau^* k/\ell^2$, dimensionless

τ^* Time, s

ψ $T - T_a/T_i - T_a$, dimensionless

ψ_a $T_b - T_a/T_i - T_a$, dimensionless

Subscripts

∞ Reservoir

b Building

i Initial

a Ambient

Superscripts

$\hat{}$ Normalized by L

Footnote p. 2
*The type of thermal diode discussed here should not be confused with that studied in the past by Buckley (Ref. 2) and others, wherein a mechanical check valve was installed into a flowing stream to prevent reverse flow. Here the geometry of the diode itself is used to eliminate reverse flow.

Footnote p. 3
*In addition, as indicated by Maloney (Refs. 5 and 8), for convective diodes using water as the working fluid, a third phase of operation exists when, during cool-down, the temperature of the cooled surface is reduced below that at which the density of water is maximized. During this phase, convection opposite to that during warm-up is believed to occur and, thus, prevent freezing of the cooled surface. This feature is useful for applications in climates where freezing nighttime conditions are common.

Footnote p. 4
*Sufficient space remains between the tongue and reservoir for a layer of insulation to thermally isolate the cool tongue from the warm reservoir.

Footnote p. 16
*One method to do this proceeds by initially assuming a value for q_L/q_n in Eq. (20) and solving for $\psi(\eta, \tau)$. After obtaining the expression for q_L/q_n from Eq. (17), substitute the result $\psi(\eta = 1, \tau)$ into it to obtain an improved estimate of q_L/q_n. This is substituted into Eq. (20) and the procedure repeated until suitable convergence is achieved.

FIGURE CAPTIONS

Fig. 1. Diode geometry.

Fig. 2. Diode geometry proposed by Maloney (Refs. 6 and 7).

Fig. 3. Thermocouple rake used in diode. Upper part is shown in this figure. Thermocouples are numbered as shown.

Fig. 4. Thermocouple rake used in diode. Lower part is shown in this figure.

Fig. 5. Boundary layer flow over irradiated diode tongue with heat losses to the outside temperature

Fig. 6. Variables used in heat transport models.

Fig. 7. Temperature in reservoir during warm-up. Heat flux to tongue is 750 W/m^2.

Fig. 8. Temperature history along horizontal plane in reservoir during cool-down.

Fig. 9. Temperature histories at four vertical locations in reservoir during cool-down. Solid lines are experimental data and symbols are calculated results.

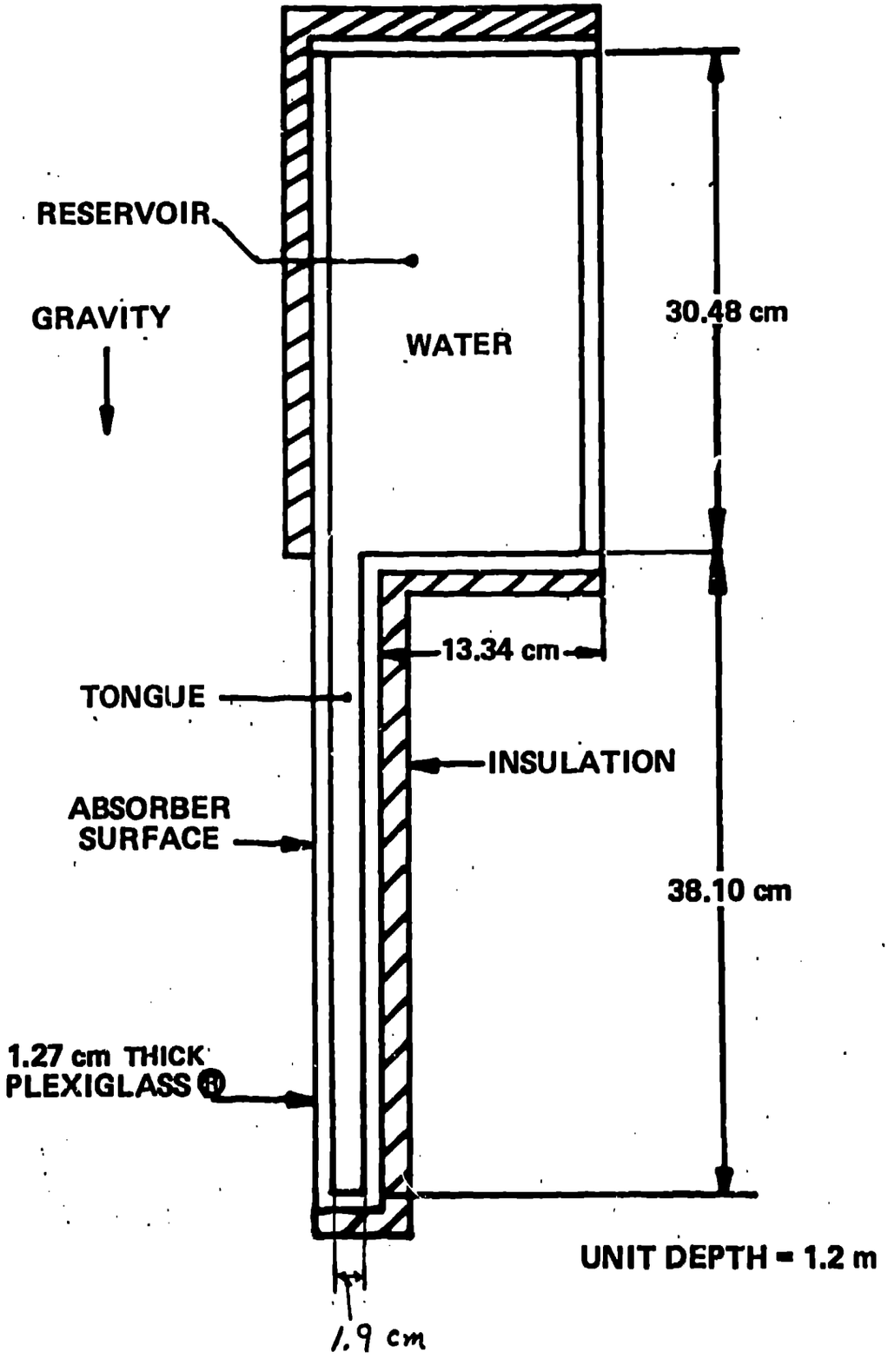
RESERVOIR
GRAVITY
WATER
30.48 cm
13.34 cm
TONGUE
INSULATION
ABSORBER SURFACE
38.10 cm
1.27 cm THICK PLEXIGLASS
UNIT DEPTH = 1.2 m
1.9 cm

Fig. 1.

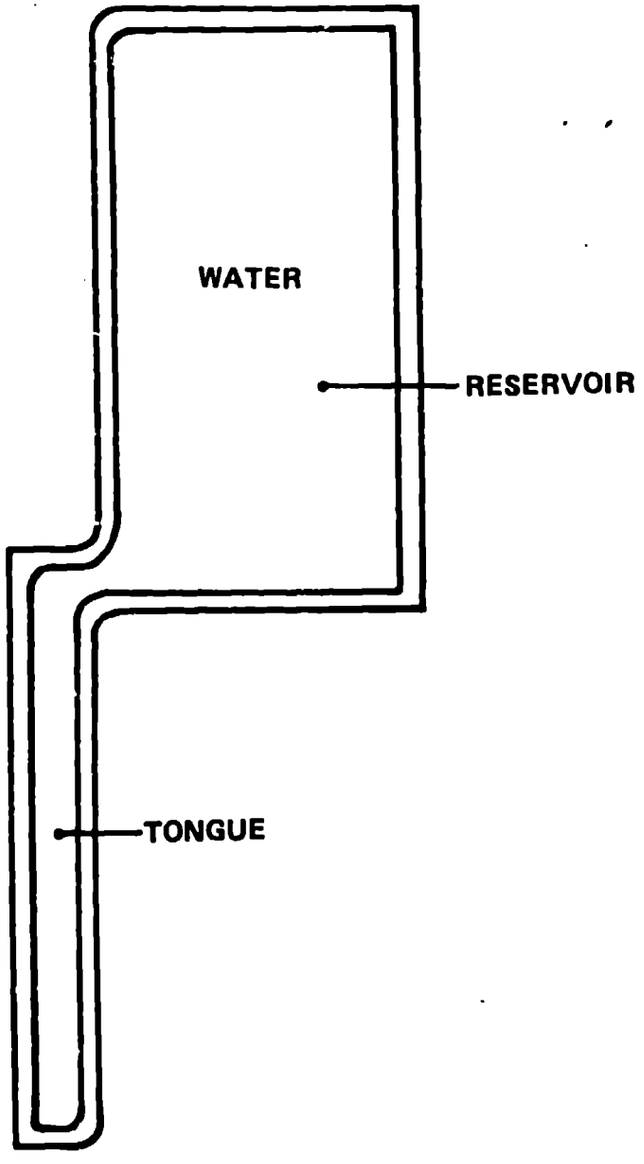

Fig. 2.

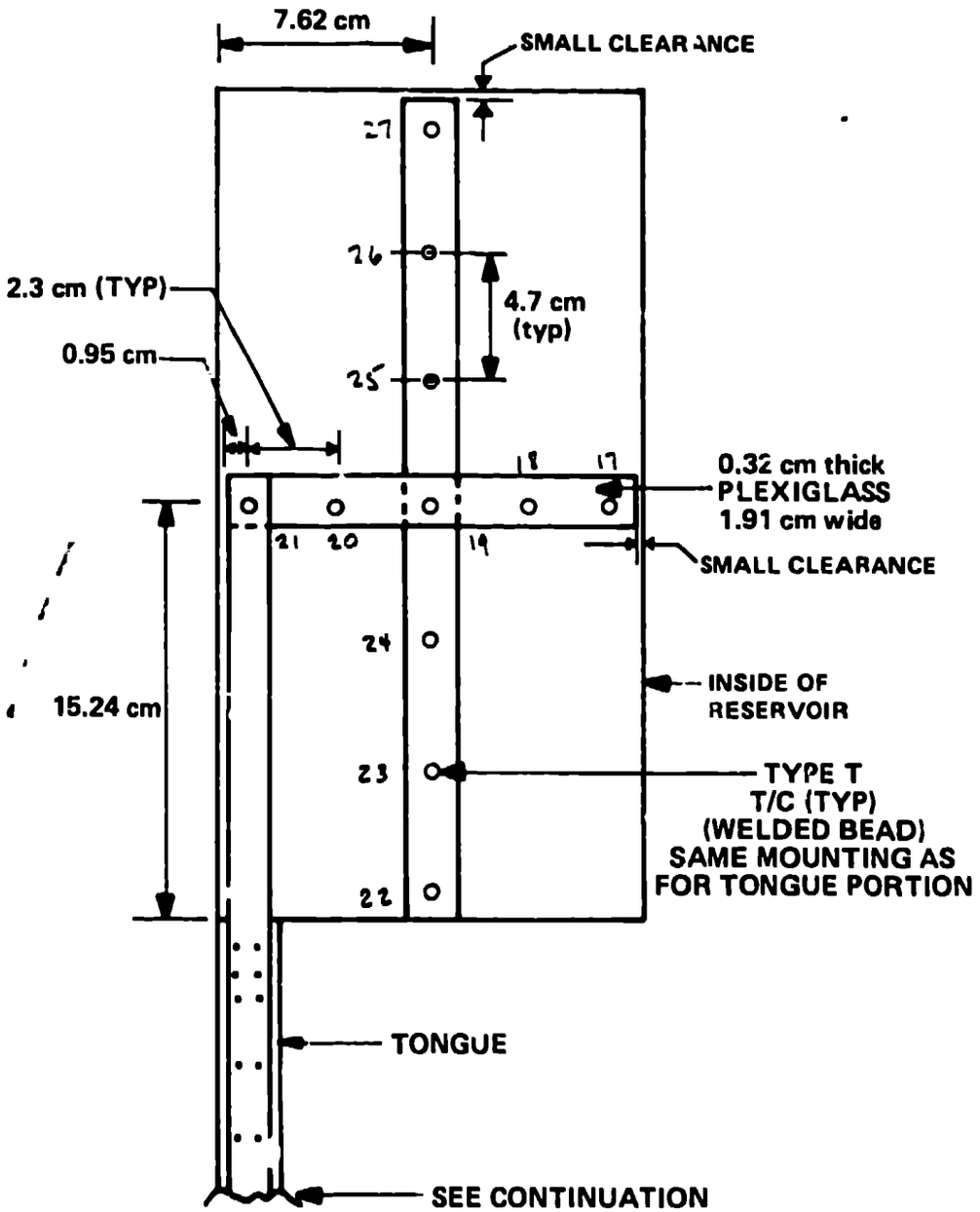
7.62 cm
SMALL CLEARANCE
27
26
25
4.7 cm
(typ)
2.3 cm (TYP)
0.95 cm
18
17
0.32 cm thick
PLEXIGLASS
1.91 cm wide
21
20
19
SMALL CLEARANCE
15.24 cm
24
INSIDE OF
RESERVOIR
23
TYPE T
T/C (TYP)
(WELDED BEAD)
SAME MOUNTING AS
FOR TONGUE PORTION
22
TONGUE
SEE CONTINUATION

Fig. 3.

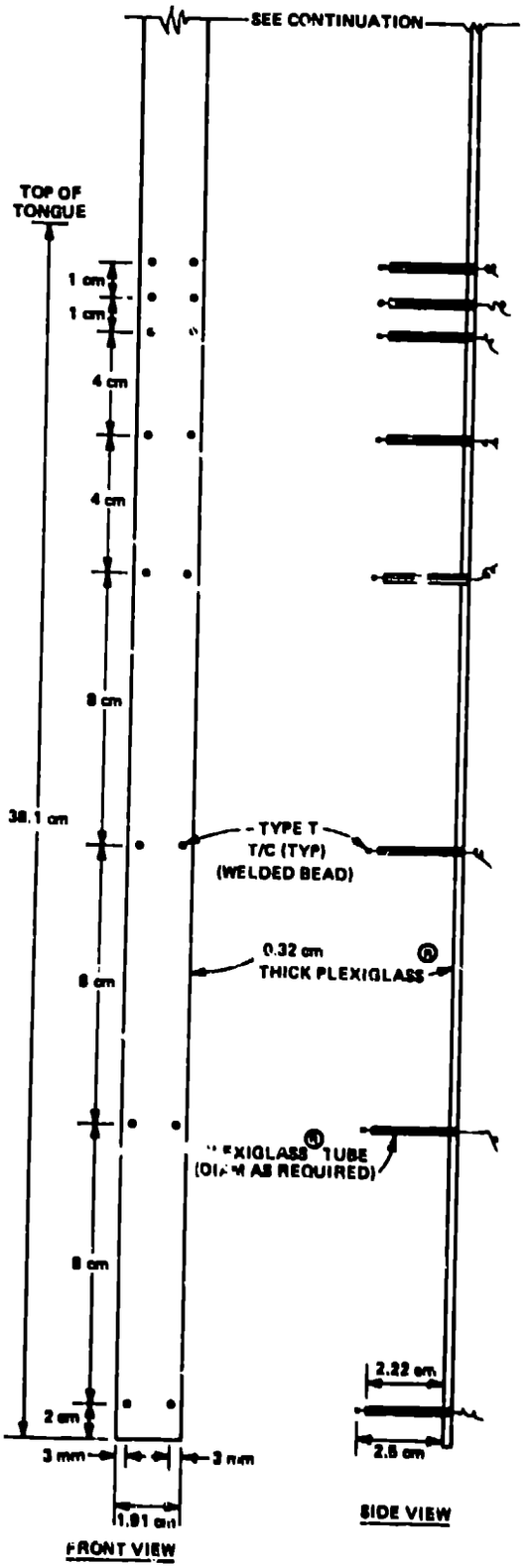
SEE CONTINUATION
TOP OF TONGUE
1 cm
1 cm
4 cm
4 cm
8 cm
38.1 cm
8 cm
8 cm
2 cm
TYPE T T/C (TYP) (WELDED BEAD)
0.32 cm THICK PLEXIGLASS®
" EXIGLASS® TUBE (DIAM AS REQUIRED)
3 mm
3 mm
1.91 cm
FRONT VIEW
2.22 cm
2.5 cm
SIDE VIEW

Fig. 4.

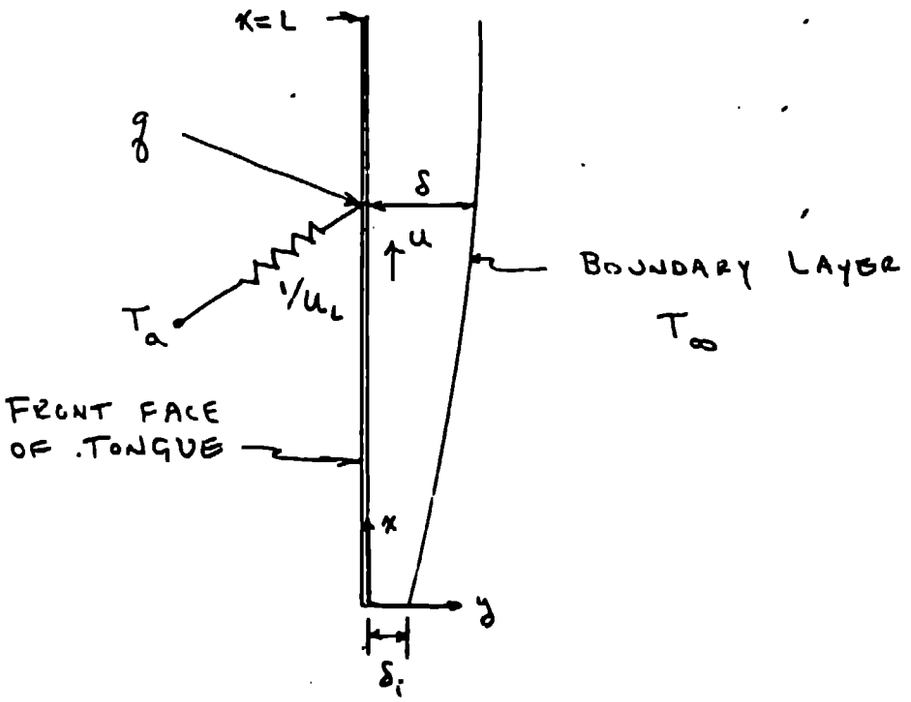
x=L
q
δ
u
BOUNDARY LAYER
T_∞
T_a
$1/U_L$
FRONT FACE
OF TONGUE
x
y
δ_i

Fig. 5.

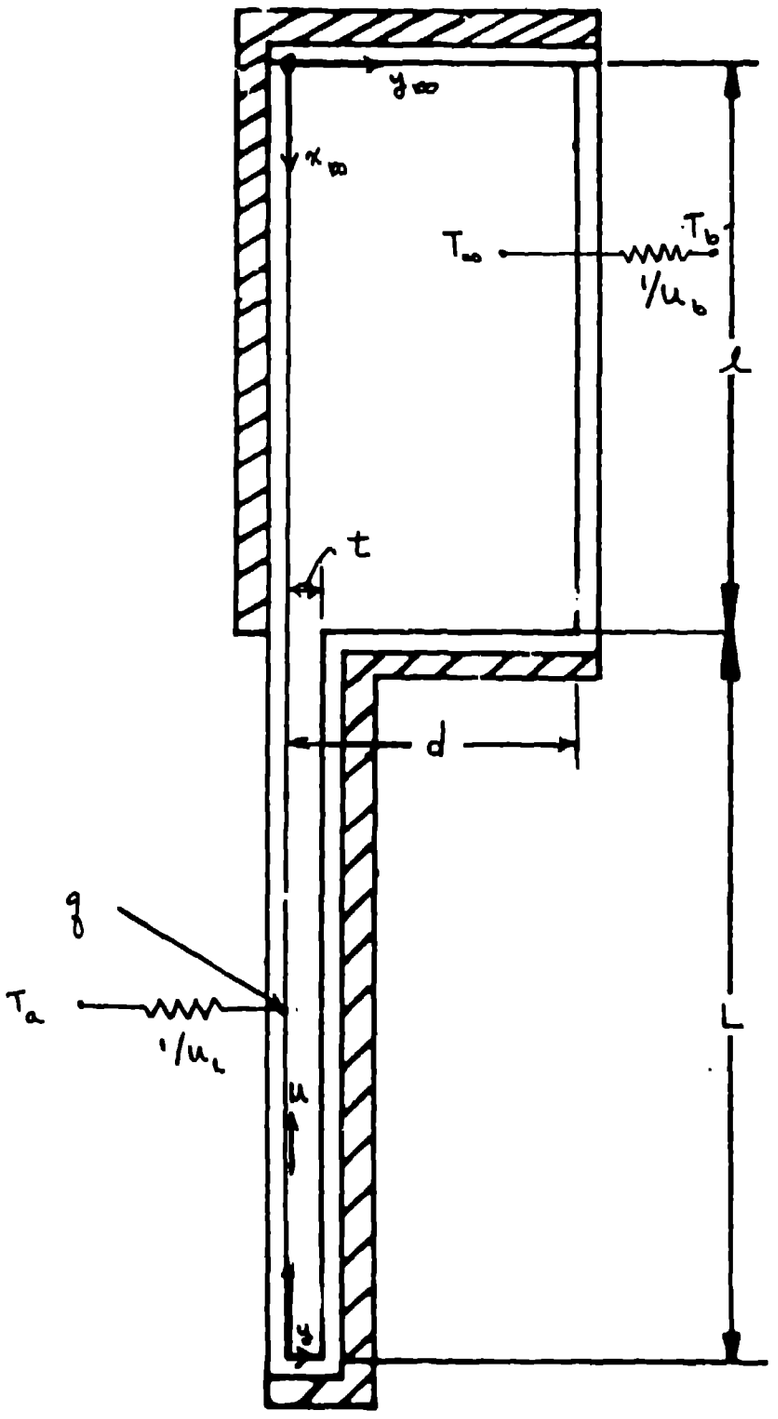

Fig. 6.

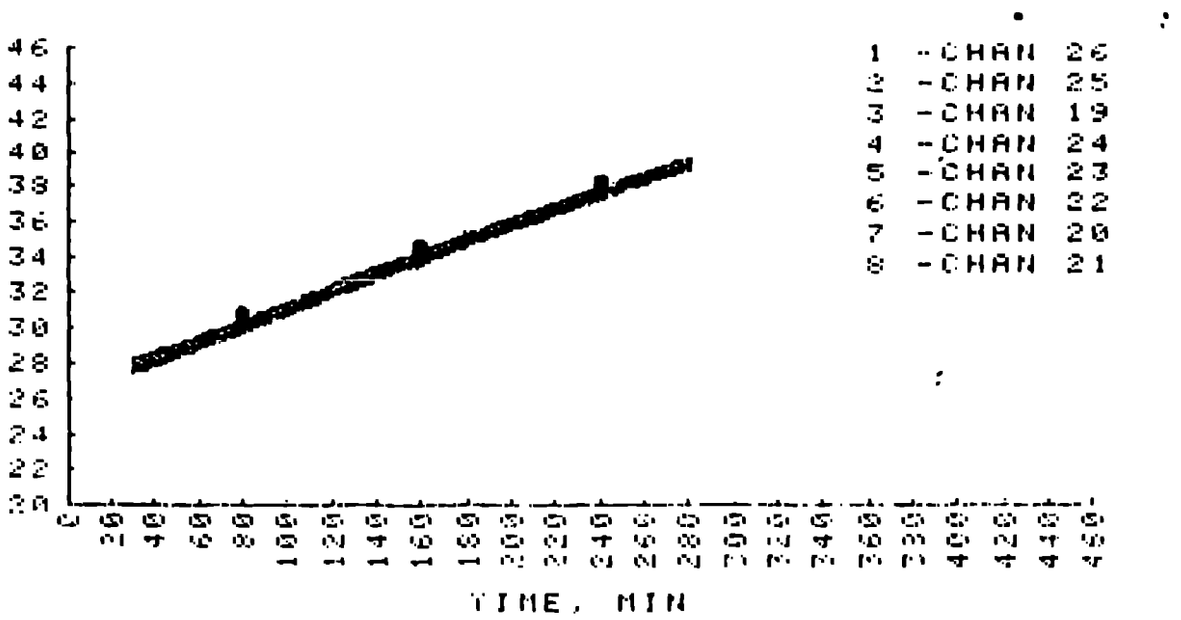
1 -CHAN 26
2 -CHAN 25
3 -CHAN 19
4 -CHAN 24
5 -CHAN 23
6 -CHAN 22
7 -CHAN 20
8 -CHAN 21
TIME, MIN

Fig. 7.

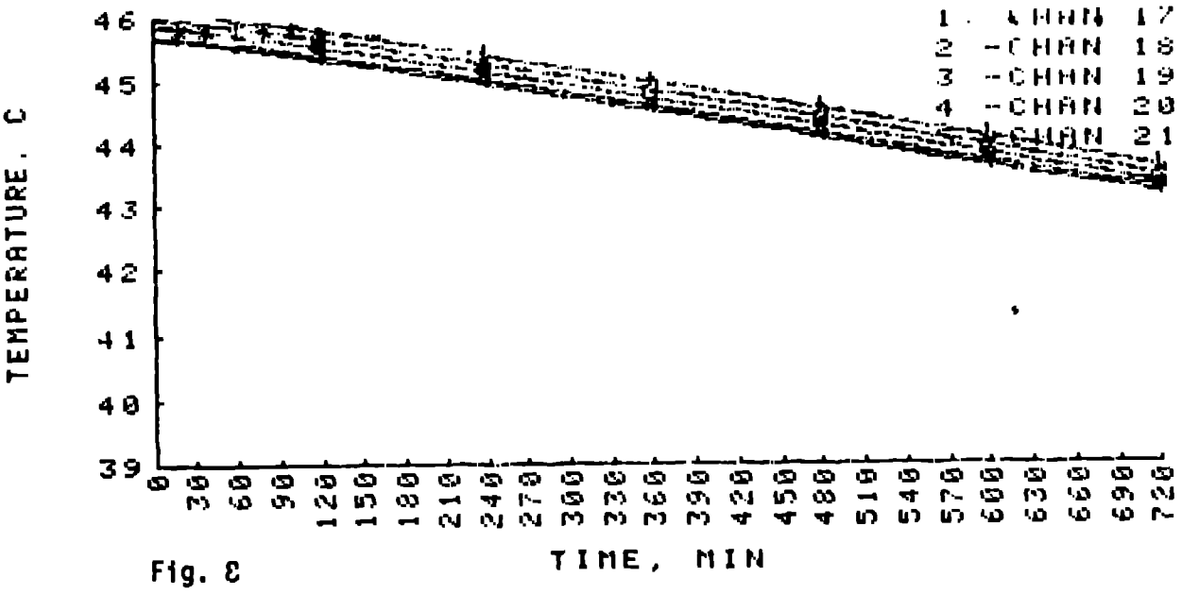
1 - CHAN 17
2 - CHAN 18
3 - CHAN 19
4 - CHAN 20
5 - CHAN 21
TEMPERATURE, C
46
45
44
43
42
41
40
39
0
30
60
90
120
150
180
210
240
270
300
330
360
390
420
450
480
510
540
570
600
630
660
690
720
TIME, MIN

Fig. 8

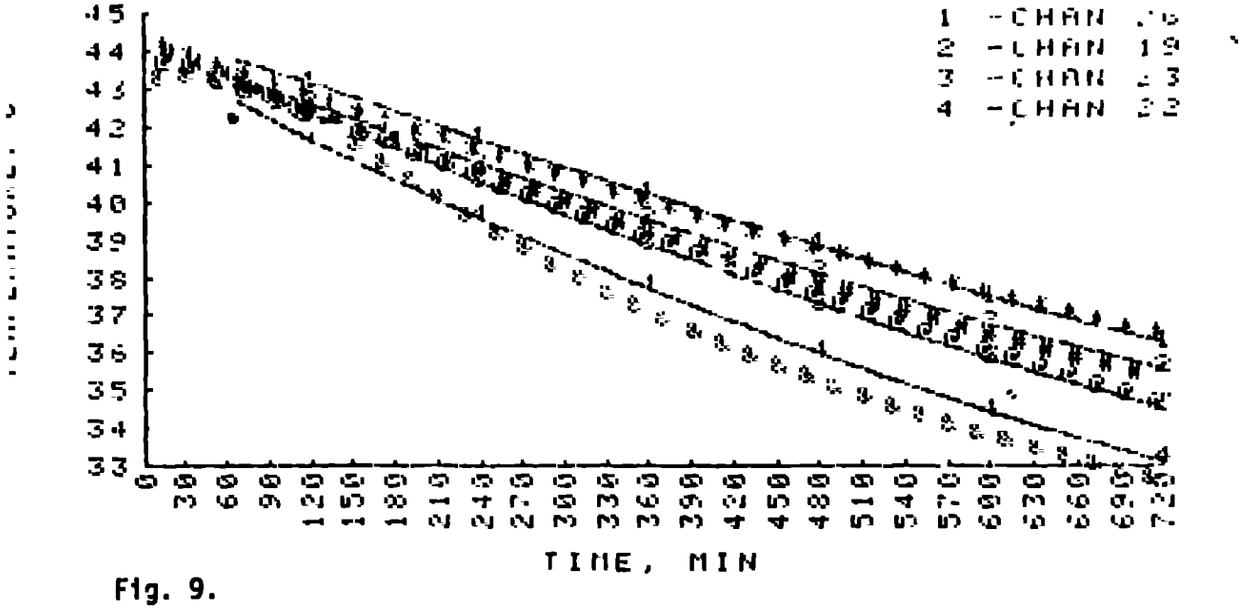
1 -CHAN
2 -CHAN 19
3 -CHAN
4 -CHAN
45
44
43
42
41
40
39
38
37
36
35
34
33
0
30
60
90
120
150
180
210
240
270
300
330
360
390
420
450
480
510
540
570
600
630
660
690
TIME, MIN

Fig. 9.